redin Revista Facultad de Ingeniería, Universidad de Antioquia, No. 77, pp. 143-152, 2015

An optimal high thermal conductive graphite microchannel for electronic device cooling

Microcanal óptimo de grafito de alta conductividad térmica para el enfriamiento de componentes microelectrónicos

Jorge Mario Cruz-Duarte*, Iván Mauricio Amaya-Contreras, Carlos Rodrigo Correa-Cely

Escuela de Ingenierías Eléctrica, Electrónica y de Telecomunicaciones, Universidad Industrial de Santander. Carrera 27 Calle 9. A. A. 678. Bucaramanga, Santander.

ARTICLE INFO

Received April 27, 2015
Accepted September 07, 2015

KEYWORDS

Microchannels, heat sinks, minimum entropy generation, unified particle swarm optimization, high thermal conductive graphite

Microcanales, disipadores de calor, mínima generación de entropía, optimización por enjambre de partículas unificado, grafito de alta conductividad térmica

ABSTRACT: This article describes the design of an optimal rectangular microchannel made of a high thermal conductive graphite (HTCG). For simulating the proposed microchannel heat sink, the total resistance model and the entropy generation minimization criterion were used. For solving the optimization problem, the unified particle swarm optimization algorithm (UPSO), was used. Results showed a marked effect of using this high thermal conductor when compared to traditional materials, such as aluminum, and while using air and ammonia gas as the working fluids. It is also reported the relative effect of the constriction, convective and fluid thermal resistances on the overall equivalent thermal resistance. As a demonstrative example when changing the nature of the coolant, a titanium dioxide nanofluid was selected. It was found that the Nusselt number is perceptibly lower, when the coolant is a nanofluid and the material for the making of the microchannel is an HTCG.

RESUMEN: Este artículo describe el diseño de un microcanal rectangular óptimo, construido con grafito de alta conductividad térmica (HTCG). Para simular el disipador de microcanales propuesto se utilizó el modelo de resistencia térmica total y el criterio de minimización de la generación de entropía. Para solucionar el problema de optimización, se utilizó el algoritmo de enjambre de partículas unificado (UPSO). Los resultados mostraron un efecto marcado al utilizar este conductor térmico, en comparación con materiales tradicionales (tales como aluminio), y utilizando aire y amoniaco gaseoso como fluidos de trabajo. También se reporta el efecto relativo de las resistencias térmicas de constricción, de convección y del fluido, sobre la resistencia térmica equivalente total. Como un ejemplo demostrativo del efecto causado al cambiar la naturaleza del refrigerante, se seleccionó un nanofluido de dióxido de titanio. Se encontró que el número de Nusselt es perceptiblemente menor, cuando se utiliza un nanofluido como refrigerante y cuando el material con que está construido el microcanal es HTCG.

1. Nomenclature

A	Area (m^2)
A_{ef}	Effective area to convective heat transfer
c_p	Average specific heat ($\mathrm{J/kg \cdot K}$)
D_h	Hydraulic diameter $\equiv 4H_c w_c/(H_c + 2w_c)$ (m)
D_{tu}	Inner diameter of the supply tubes (m)
EGM	Entropy Generation Minimization
f	Darcy friction factor
G	Volume flow rate (m^3/s)
$\boldsymbol{G}_p$	Global velocity component of a particle
$\bar{h}$	Average convection coefficient ($\mathrm{W/m^2 \cdot K}$)
HTCG	High Thermal Conductive Graphite
H_c	Channel height (m)
k	Thermal conductivity of solid ($\mathrm{W/m \cdot K}$)
k_f	Thermal conductivity of fluid ($\mathrm{W/m \cdot K}$)
L	Length (m)
$\boldsymbol{L}_p$	Local velocity component of a particle
N_c	Total number of microchannels
Nu_{D_h}	Nusselt number base on hydraulic diameter $\equiv \mathrm{D_h \bar{h}/k_f}$
P	Pressure (Pa)
Pe_{D_h}	Péclet number base on hydraulic diameter $\equiv \mathrm{D_h \bar{V}_f/\alpha_{th}}$
$\boldsymbol{P}_g$	Best position of the swarm
$\boldsymbol{P}_{g_p}$	Best position found by each neighborhood
$\boldsymbol{P}_p$	Best solution found by each particle
Pr	Prandtl number $\equiv c_p \mu/k_f$
$\dot{q}$	Uniform heat flux ($\mathrm{W/m^2}$)
$\dot{Q}$	Total heat transfer rate (W)

* Corresponding author: Jorge Mario Cruz Duarte
e-mail: jorge.cruz1@correo.uis.edu.co
ISSN 0120-6230
e-ISSN 2422-2844

DOI: 10.17533/udea.redin.n77a17

R	Thermal resistance (K/W)
Re_{D_h}	Reynolds number base on hydraulic diameter ≡ $D_h \bar{V}_f / \nu$
$\dot{S}_{gen}$	Total entropy generation rate (W/K)
$\dot{S}_{gen,\Delta P}$	Entropy generation rate due to mass flow (W/K)
$\dot{S}_{gen,\Delta T}$	Entropy generation rate due to heat transfer (W/K)
t	Actual iteration or step
t_b	Lower plate thickness (m)
T	Average temperature (K)
u	Unification factor
UPSO	Unified Particle Swarm Optimization
$\bar{V}_f$	Average velocity of the fluid through channels (m/s)
$\boldsymbol{V}_p$	Total velocity of a particle
w_c	Half of the channel width (m)
w_p	Half of the fin thickness (m)
W	Width (m)
$\mathbf{x}$	Design variable
$\boldsymbol{X}_p$	Position of a particle

Greek symbols

α_c	Channel aspect ratio ≡ $2w_c/H_c$
β	Channel-wall ratio ≡ w_c/w_p
ΔP	Pressure drop across microchannel (Pa)
ΔT	Finite temperature difference (K)
η_p	Efficiency of the wall
λ	Mean free path (m)
μ	Dynamic viscosity of fluid (Pa · s)
ν	Kinematic viscosity of fluid (m^2/s)
ρ	Average density of fluid (kg/m^3)
ϕ_1	Own trust factor
ϕ_2	Swarm trust factor
Φ	Total pump power
χ	Constriction factor
Ψ	Search agents population

Subscripts

a	Surrounding or ambient
b	Base plate
c	Channel
$conv$	Convection
$const$	Constriction
CV	Control volume
d	Heat sink
eq	Equivalent
f	Fluid
i	Interface
ghs	Geometrical properties of the heat sink
pf	Parameter of the fluid
$phsf$	Parameter depending on both, the heat sink and the fluid
ths	Thermal properties of the heat sink
tpf	Thermal property of the fluid
tu	Supply pipes of fluid flow

2. Introduction

There are plenty of literature reports regarding simulation and experimental results of different approaches for the optimal design of heat sinks used for a suitable thermal management of electronic components. Through them, designers must select the material for making the required heat sink, the type of coolant, the operating conditions that best match the requirements, and the overall cost of the implementation, principally. Each of the above mentioned options has several alternatives, e.g. the shape of the heat sink, the physicochemical characteristics of the heat sink surface, the physicochemical properties of the working fluid and its flow regime, the convective heat transfer coefficient, and so on. For the present study, it was of interest to find a commercially available material with high thermal conductivity for building microchannel heat sinks. Alas, an extensive literature review revealed few materials with these characteristics. There is now, for example, accessible Oxygen Free High thermal Conductivity copper (OFHC) (k=400 W/m·K). As stated in [1], the thermal conductivity of crystalline graphite could reach values of the order of 3000 W/m·K. More recently, synthetically made high thermal conductive graphite (HTCG) was developed from a highly oriented graphite polymer film [2]. It has thermal conductivities of the order of 1300-1900 W/m·K. Furthermore, it can be composited with conventional polymers, in order to get microchannel heat sinks with different shapes and required thermal conductivities and densities, more easily. In [3] is reported an investigation related to the measurement of the thermal conductivity of graphene suspended across channels in a Si/SiO_2 wafer. They claimed extremely high thermal conductivity, in the range of 3080–5150 W/m·K, for this material. In [4], it was prepared composite phase change materials (PCM) using exfoliated graphite nanoplateles (xGnP), paraffin/xGnP with high electric and thermal conductivity. The thermal conductivity of the composite increased with the xGnP loading. [5] describes the preparation of a high thermal conductive thin graphite film with a thickness about 2.1 μm using a thin polymer film as a start material. The a-b plane thermal diffusivity of the film was measured. They obtained a graphite film composed of highly oriented graphite layers in a-b plane. Similarly, [6] describes the fabrication of graphite flake reinforced copper composites. The composite materials prepared with 40 vol. % graphite flakes showed a strong anisotropy in thermal conductivity and values, as high as, 528 W/m·K at room temperature. Lately, [7] studies the thermal conductivity of shape-stabilized phase-change materials (PCM) for thermal energy storage, based on a soft Fischer–Tropsch paraffin wax blended with ethylene vinyl acetate (EVA). In the same direction, [8] prepared composites made of expanded graphite (EG) and eutectic water solutions of $NaNO_3$-$LiNO_3$, in order to increase the thermal conductivity of high-temperature phase change materials, or PCMs. As he states, a higher graphite percentage (10-30%) progressively increases the thermal conductivity of the composite, with intensifications up to 10. Finally, [9] studied the heat transfer properties of a PCM made of squama expanded graphite (EG) and paraffin. Because of its composition, this kind of

material has a high anisotropic thermal conductivity. Their results show that the anisotropic property of the thermal conductivity of the composite PCM is obvious, and the temperature curves are deflexed and scattered during the apparent heat transfer process of the PCMs of liquid state.

It is also known from previous works, that rectangular microchannels provide the best thermal performance with lower thermal resistance [10, 11]. In fact, several researchers report simulation data using this type of microchannels, but with different working fluids, such as water, air, nitrogen, and argon, among several others. Particularly, in [10] it was reported the potential improvement in the overall performance of a rectangular microchannel heat sink using ammonia gas as a coolant. From the simulation point of view, as was mentioned earlier in [12], literature reports several strategies for modeling this type of heat transfer problem, such as the thermal resistance model, fin model, two fin-fluid coupled models, and porous medium model, principally. Several researches have recently started to explore different alternatives not only to construct and to solve the mathematical model, but also to design an optimal heat sink that maximizes the heat transfer process. From all the analytical resources available for designing purposes, the Entropy Generation Minimization (EGM) criterion is the highest disseminated and illustrated in the literature. It is because of its sound thermodynamics basis. The EGM can be applied to each component of a thermodynamic system and it takes into account the irreversibility due to fluid flow, e.g. pressure drop, and the irreversibility due to heat transfer, e.g. heat transfer between finite temperature differences. Hence, it is possible to build an objective function that represents the sum of all components, so appropriate design parameters can be found that guarantee the maximum efficiency of the whole system. The present article summarizes results from several simulation scenarios for designing, based on the EGM criterion, an optimal rectangular microchannel heat sink made of high thermal conductive graphite. Its behavior was compared against a heat sink made of aluminum. Likewise, two working fluids in gas phase were studied: dry air and ammonia gas. In addition, some simulations using water and a nanofluid composed of titanium dioxide nanoparticles and water were done for comparison purposes. This paper begins by briefly describing the mathematical model and the optimization strategy used in the current work, followed by a summary of the methodology, and a discussion of the results. Finally, the main conclusions are laid out.

3. Mathematical model

The general deduction of the mathematical model of a similar system was previously presented in some detail in [12]. Subsequently, its most remarkable aspect is described. Figure 1 shows an overview of the model system, including a layer of thermal paste between the heat sink and the chip. The former, is made up of N_c channels with the following specifications: width $2W_c$, height H_c, length l_d, separated by walls (fins) with a thickness $2w_p$. The total dimensions of the heat sink are $W_d \times L_d \times H_c$, and it is limited by two parallel plates at the top and bottom faces of the fin array. The lower plate has a thickness t_b and an area $W_d \times L_d$.

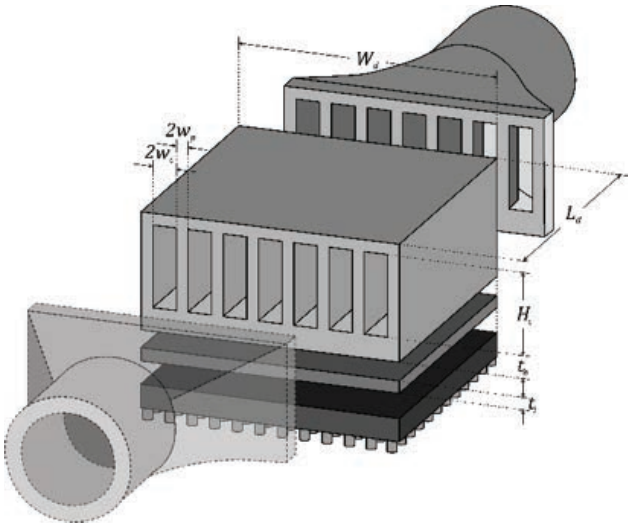

Figure 1 System under study: microchannel heat sink and its interface

3.1. Total entropy generation rate

In order to model the system (Figure 1) in terms of entropy generation, a representative control volume must be analyzed in terms of mass, energy and entropy balances [13]. Because of symmetry, the control volume (*CV*) is defined as half a channel of the heat sink, with dimensions $(w_c + w_p) \times (H_c + t_b + t_i) \times L_d$, with a uniform heat flux $\dot{q}$ that enters through the bottom plate. Hence, entropy generation rate is given by (1), where the finite temperature difference between the boundary temperature (t_i), and the surrounding temperature (t_a), is ΔT ($=T_i - T_a$). Heat transfer rate $\left(\dot{Q}_{CV} = \dot{q} \cdot (w_c + w_p) L_d\right)$, volume flow rate ($G_{CV}$) and pressure drop ($\Delta P$) are also included in this equation. After finding $\dot{S}_{gen,CV}$ in (1), the total entropy generation rate $\left(\dot{S}_{gen}\right)$ is found by symmetry [14].

$$\dot{S}_{gen,CV} = \frac{\Delta T}{T_i T_a} \dot{Q}_{CV} + \frac{\Delta P}{T_a} G_{CV} \qquad (1)$$

The model given in (2), is defined in terms of the entropy generated due to the irreversibility of heat transfer $\left(\dot{S}_{gen,\Delta T}\right)$ and mass flow $\left(\dot{S}_{gen,\Delta P}\right)$, both of them present during the operation of the whole system. In (2), factor $R_{eq}\ (= \Delta T / \dot{Q}_d)$ relates to the equivalent thermal resistance of the whole heat sink, while factor $\dot{Q}_d\ (= \dot{q} \cdot W_i L_i)$ relates to the net power dissipated by the chip; G_d represents the net fluid flow, and $N_c\ (= (W_d/2 - w_p)/(w_c + w_p))$ is the number of microchannels in the heat sink.

$$\dot{S}_{gen} = \frac{\dot{Q}_d^2}{T_a T_i} R_{eq} + \frac{G_d}{T_a} \Delta P$$
$$= \dot{S}_{gen,\Delta T} + \dot{S}_{gen,\Delta P} \quad (2)$$

Additionally, $\dot{S}_{gen}$ can be expressed in terms of the wasted available work (or destroyed exergy) as shown in (3), where Φ ($= G_d \Delta P$) is the total pump power required to maintain the fluid flow. The expressions for calculating R_{eq} and ΔP, based on the previously shown operating conditions, are discussed next.

$$T_a \dot{S}_{gen} = \frac{\dot{Q}_d^2 R_{eq}}{T_i} + G_d \Delta P \quad (3)$$

3.2. A simplified equivalent thermal resistance model

For the present case, the equivalent thermal resistance of the heat sink (R_{eq}) can be modeled through an analogy to electric circuits, where the heat flux ($\dot{Q}$) relates to the electrical current and the finite temperature difference corresponds to the potential difference. Hence, in order to find R_{eq} the resistive components related to material changes and heat transfer must be known. This is shown in (4), where R_{const}, R_{conv} and R_f are the resistances due to conduction through the microchannel body, convection on the channels, and calorific capacity of the working fluid, respectively.

$$R_{eq} = \frac{T_b - T_a}{\dot{Q}_d} = \frac{T_b - T_s}{\dot{Q}_d} + \frac{T_s - T_f}{\dot{Q}_d} + \frac{T_f - T_a}{\dot{Q}_d}$$
$$= R_{const} + R_{conv} + R_f \quad (4)$$

The spreading thermal resistance is not considered in this model, i.e., the area available for heat transfer between the base of the heat sink and the chip are assumed to be equal. We have also neglected the other thermal resistances, such as that due to the thermal paste, for example, in order to simplify the analysis. The average temperatures given in (4) relate to those of the base surface (T_b), of the surface contacting the fluid (T_s),and of the fluid outlet (T_f) and inlet (T_a). The constriction thermal resistance, R_{const}, due to heat transfer through the microchannel body is given by (5). Now, using Newton's cooling law, an expression for R_{conv} is given by (6).

$$R_{const} = \frac{w_p + w_c}{\pi k W_d L_d} ln\left[sin\left(\frac{\pi w_p}{2(w_p + w_c)}\right)\right]^{-2} \quad (5)$$

$$R_{conv} = \frac{T_s - T_f}{\dot{Q}_d} = \frac{1}{\bar{h} A_{ef}}; \quad A_{ef} = 2N_c L_d \cdot (w_c + \eta_p H_c) \quad (6)$$

This agrees to the expression found by [13], where $\bar{h}$ is the average convection coefficient and η_p is the thermal efficiency of the fin. Coefficient $\bar{h}$ relates to Nusselt number (Nu_{D_h}), to the thermal conductivity of the fluid k_f, and to the effective hydraulic diameter of the channel D_h ($= 4w_c H_c/(2w_c + H_c)$). The efficiency η_p, is evaluated through (7), where m is the fin parameter that depends on the geometry of the fin, and on coefficients $\bar{h}$ and k. The latter is the thermal conductivity of the heat sink. Finally, the resistance of the working fluid can be found through an energy balance at the fluid flow, yielding (8).

$$\eta_p = \frac{tanh(mH_c)}{mH_c}; \; m = \left[\frac{2(w_p + L_d)}{w_p L_d}\right]^{0.5} \cdot \left[\frac{\bar{h}}{k}\right]^{0.5} \quad (7)$$

$$R_f = \frac{T_f - T_a}{\dot{Q}_d} = \frac{1}{G_d}\left[\frac{1}{\rho c_p}\right]_f \quad (8)$$

Summarizing, the equivalent thermal resistance of the whole heat sink, defined in (4), is rewritten in (9) as,

$$R_{eq} = \left\{\left[\frac{w_p + w_c}{\pi W_d L_d}\right] ln\left[sin\left(\frac{1}{2}\frac{\pi w_p}{(w_p + w_c)}\right)\right]^{-2}\right\}_{ghs}\left[\frac{1}{k}\right]_{ths}$$
$$+ \left[(2N_c L_d w_c)_{ghs}(\bar{h})_{phsf} + (2N_c L_d H_c)_{ghs}(\eta_p \bar{h})_{phsf}\right]^{-1}$$
$$+ \left[\frac{1}{G_d}\right]_{pf}\left[\frac{1}{\rho c_p}\right]_{tpf} \quad (9)$$

3.3. Total pressure drop

This term, found in (2), can be determined with (10), where a relation is made between pressure drop due to load loss and to channel inlet and outlet, as a function of the average density of the fluid (ρ), of the average velocity of the fluid ($\bar{V}_f = G_d/2N_c w_c H_c$), of the Darcy friction factor (f), of the length or depth of the channel (L_d), of the hydraulic diameter (D_h), and of the relation given by β ($= w_c/w_p$), respectively [13].

$$\Delta P = \rho \frac{\bar{V}_f^2}{2}\left[f\left(\frac{L_d}{D_h}\right) + 1.79 - 2.32\left(\frac{\beta}{1+\beta}\right) + 0.53\left(\frac{\beta}{1+\beta}\right)^2\right] \quad (10)$$

In order to calculate the friction factor (f), shown in (10), the correlations given in [14] for smooth surfaces were employed. Equally, for calculating the Nusselt number, the expressions given by [15] when using gas as a working fluid, were used.

3.4. The objective function

Now, the objective function can be constructed. It compiles all of the above empirical expressions, (4)-(10), in the entropy balance, resulting in (11). To include in this optimization process the pressure drop throughout the supply pipes, several correlations were used, but they are not shown here.

$$\min\{\dot{S}_{gen}\} = \min\left\{\frac{\dot{Q}_d^2}{T_a T_i} R_{eq} + \frac{G_d}{T_a}\Delta P\right\},$$
$$\text{subject to } \frac{2w_c}{H_c} - 1 \leq 0 \text{ and } 1 - \frac{w_c}{w_p} \leq 0. \quad (11)$$

4. Optimization procedure

In order to solve the problem described in (11), many optimization techniques can be selected. A very specific method, based on swarm intelligence and widely used in several engineering applications, is Unified Particle Swarm Optimization (UPSO). UPSO was proposed by Parsopoulos and Vrahatis and it was inspired by the natural process of food search carried out by bird flocks and fish shoals. Basic equations of UPSO are shown in (12) and (13). They consider the swarm's kinematic and the movement and positioning of each individual agent of the swarm.

$$V_p^{t+1} = \chi\left[V_p^t + \varphi_1\left((1-u)\cdot rand_1 + u\cdot rand_2\right)\left(P_p - X_p^t\right) + \varphi_2\left((1-u)\cdot rand_3\left(P_g - X_p^t\right) + u\cdot rand_4\left(P_{gp} - X_p^t\right)\right)\right] \quad (12)$$

$$X_p^{t+1} = X_p^{t+1} + V_p^{t+1} \quad (13)$$

In equations (12) and (13), $\mathcal{V}_p^t$ and X_p^t are the total velocity and the position, respectively, at time step t, for a particle p in the swarm, where $p = 1, \ldots, \Psi$, and Ψ is the total number of agents. χ is the constriction factor; φ_1 and φ_2 are respectively the self and swarm confidence constants; $rand_i$ is an uniformly distributed random number between zero and one, where $i = 1, 2, 3$ and 4; $\mathcal{P}_p$, $\mathcal{P}_{gp}$ and $\mathcal{P}_g$ are the best positions found by each particle, by each neighbourhood and by the swarm, respectively.
For a defined optimization problem, $f_{obj}(X)$, UPSO pseudocode is briefly described below, using the previously mentioned equations.

1) Define $\chi, \varphi_1, \varphi_2, \Psi$ and the selection criteria of the neighbourhoods, the search domain $X_{min} \leq X_p \leq X_{max}$, and the objective function $f_{obj}(X)$.
2) Randomly assign the initial position of each particle, X_p^1, over the search domain and assign an initial value for the velocity V_p^1.
3) Evaluate each position, X_p, in f_{obj} and find $\mathcal{P}_p, \mathcal{P}_{gp}$ and $\mathcal{P}_g$.
4) Use (12) and (13) to calculate X_p^{t+1} and $\mathcal{V}_p^{t+1}$, respectively.
5) Evaluate each new position in the objective function and update $\mathcal{P}_p, \mathcal{P}_{gp}$ and $\mathcal{P}_g$.
6) Check stop criteria. If it complies, stop and print results. Otherwise, make $t = t + 1$ and go to step four.

5. Simulation methodology

Throughout this work, simulation results were obtained using a computer with the following specifications: ASUS® S46C, CPU Intel® Core™ i7-3537U @ 2.00 GHz – 2.50 GHz, 6 GB RAM, Microsoft® Windows™ 8.1 Single - 64 bits. The parameters assumed for the simulations are declared in Table 1 and the description of each one was given in the previous section. These values were found through a previous study with standard test functions that is not shown here due to space restrictions. Additionally, the data was calculated for 100 runs of each simulation. The optimization algorithm used in this work, i.e. UPSO, including the pseudocode, are fully described elsewhere [12, 16].

Table 1 Parameters used for the UPSO algorithm

Method	Parameter	Possible values	Selected value
UPSO	Ψ	25 and 100	100
	ϕ_1	2.0, 2.5 and 3.0	2.0
	ϕ_2	2.0, 2.5 and 3.0	2.5
	χ	0.6 and 0.8	0.6
	u	0.2, 0.5 and 0.8	0.5

5.1. Parameter variation

Initially, a set of simulations was conducted to show just the effect of the entropy generation due to the mass flow $(\dot{S}_{gen,\Delta P})$, i.e. assuming zero thermal resistance. This limiting case indicates the effect of the flow mass passing through the microchannel heat sink. Also, it shows the importance of the fluid and solid-fluid interphase properties. After that, another group of simulations was ran, but including this time just the thermal resistances due to the convective heat transfer mechanism and the thermal resistance, due to the fluid used as a coolant, (without including the mass flow entropy effect). Next, simulations including the denominated constriction resistance were executed. In order to compare all those effects, air and ammonia gas as coolants and rectangular microchannels

made of HTCG and aluminum were used. Table 2 shows the thermophysical properties of the bulk materials and coolants used. The following design parameters were varied through the simulation: heat sink length L_d, between 0.01 m and 1 m; channel width $2w_c$, between 100 µm and 1000 µm; and volume flow rate G_d, between 0.001 m³/s and 0.01 m³/s. The values shown in Table 3 were used to this end. A completely developed laminar regime was assumed.

Table 2 Thermophysical properties of the bulk materials and coolants considered in the simulation

Material	ρ (kg/m³)	k (W/m · K)	$\nu \times 10^{-5}$ (m²/s)	c_p (J/kg · K)
High thermal conductive graphite (HTCG)	1000	1900	-	742
Aluminum (Al)	2707	237	-	910
Air	1.1614	0.0261	1.58	1007
Ammonia gas (NH3)	0.7	0.027	1.4654	2158

Table 3 Design specifications assumed for the parameters of the heat sink [17]

Parameter	Value	Unit
L_d, L_i	50×10^{-3}	m
W_d, W_i	50×10^{-3}	m
H_c	25×10^{-3}	m
t_b	0.1×10^{-3}	m
L_{tu}	0.5	m
D_{tu}	1.9×10^{-2}	m
$\dot{q}$	50×10^{3}	W/m²
T_a	300	K
G_d	4.5×10^{-3}	m³/s

6. Results and discussion

Nomenclature used throughout this section is now presented. **M1**: represents the optimal simulation results when the entropy generation of the microchannel made of HTCG is due to the mass flow of the coolant only; **M2**: represents the optimal simulation results when the entropy generation of the microchannel made of HTCG is due to the heat transfer but including R_{conv} and R_f only; **M3**: represents the optimal simulation results when the entropy generation of the microchannel made of HTCG is due to the heat transfer but including R_{const}, R_{conv} and R_f only; **M4**: represents the optimal simulation results when the entropy generation of the microchannel made of HTCG is due to the two contributions, i.e., the thermal and the mass flow effects. R_{const}, R_{conv} and R_f are included. Figure 2a compiles the simulation results for the case dry air-HTCG. As can be observed, each of the limiting cases complies with the expected results. Increasing G_d, the entropy generation due to the mass flow of the coolant increases continuously. On the other hand, due to the high thermal conductivity of the graphite, its effect on the total thermal resistance is negligible and imperceptible at the scale shown. Nevertheless, increasing the mass flow of the working fluid the thermal resistance R_f decreases while keeping constant the other two. The total entropy generation has a minimum value too. When using ammonia gas as the working fluid and keeping the same microchannel made of HTCG, as shown in Figure 2b, the simulation results changed indicating the importance of the physicochemical properties of the working fluid and their effects on the average convective heat transfer coefficient. Nonetheless, previously discussed trends are preserved.

Now, changing to aluminum, i.e. the material which is made of the rectangular microchannel, and keeping dry air as the coolant, the simulation results are quite similar to

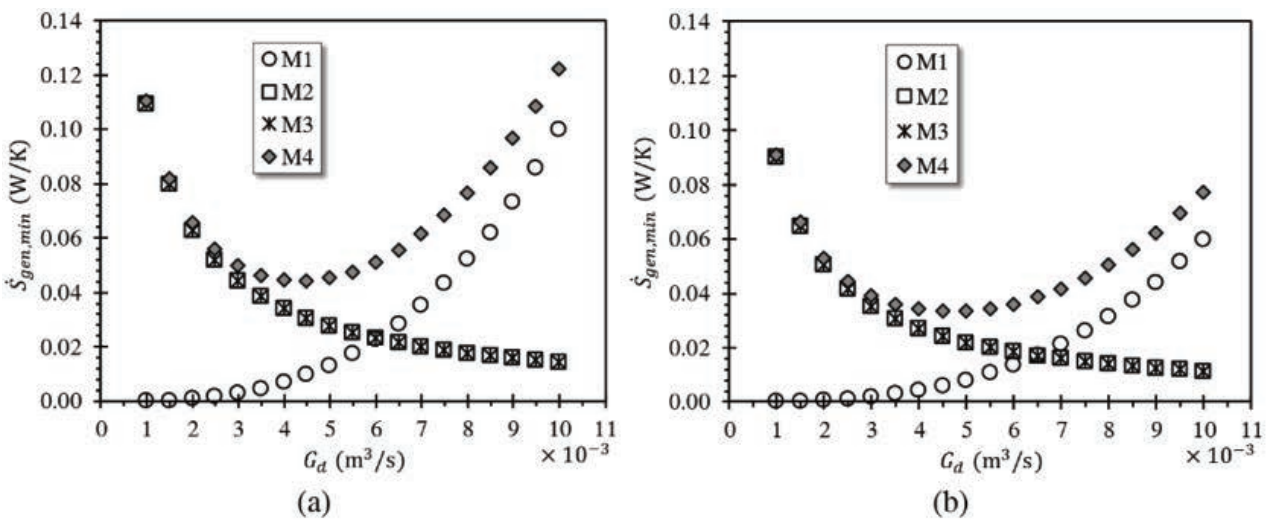

Figure 2 Entropy generation as a function of the volumetric flow of the coolant, for the case: (a) dry air-HTCG, and, (b) ammonia gas-HTCG

those shown in Figure 2, as observed in Figure 3a. Figure 3b depicts the behavior of the same system, but now using ammonia gas as the coolant for the same aluminum rectangular microchannel. As before, the same trends are observed. It was also evident that the entropy generation was consistently lower than the shown in Figure 4a. From the simulation point of view, it seems plausible to think that the overall phenomena controlling the heat transfer process, for the present case, is now changing to the side of the fluid instead to the material which the microchannel is made of. The thermal conductivity of the HTCG used in the simulations was of the order of 1900 $\mathrm{W/m \cdot K}$. Using, for example, materials with higher thermal conductivity such as graphene flakes (3080–5150 $\mathrm{W/m \cdot K}$) would render R_{const} to practically zero, but the total thermal resistance will still be dependent on R_{conv} and R_f. After several simulations, it was observed the relative importance of the three thermal resistances considered here on the overall heat transfer process.

For all cases, the constriction thermal resistance represented less than 0.15% of the total equivalent thermal resistance, as depicted in Figure 4.

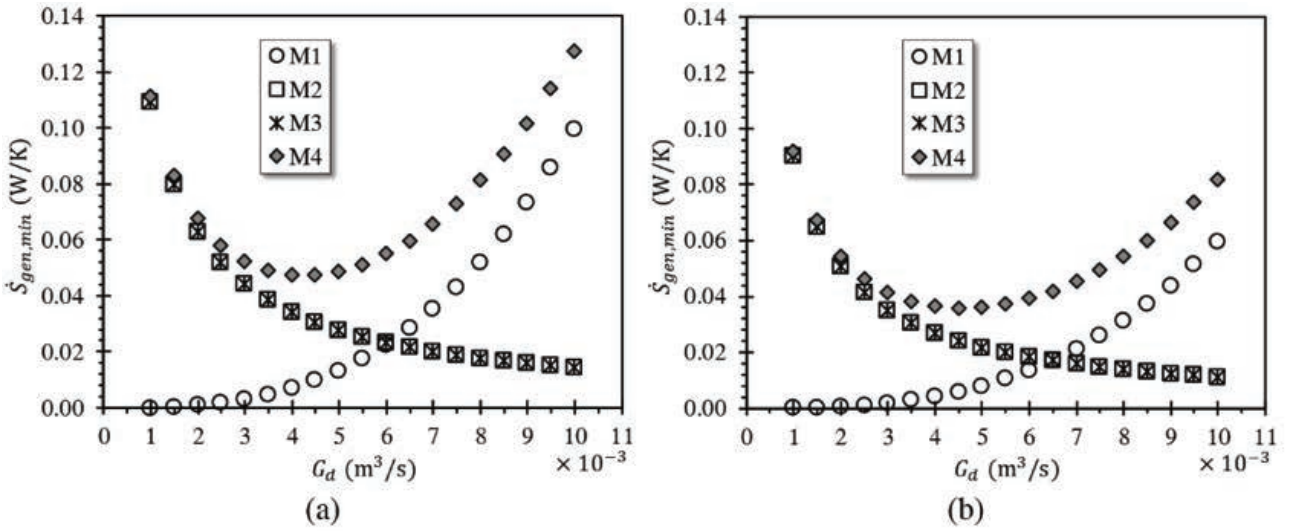

Figure 3 Entropy generation as a function of the volumetric flow of the coolant, for the case: (a) dry air-aluminum, and, (b) ammonia gas-aluminum

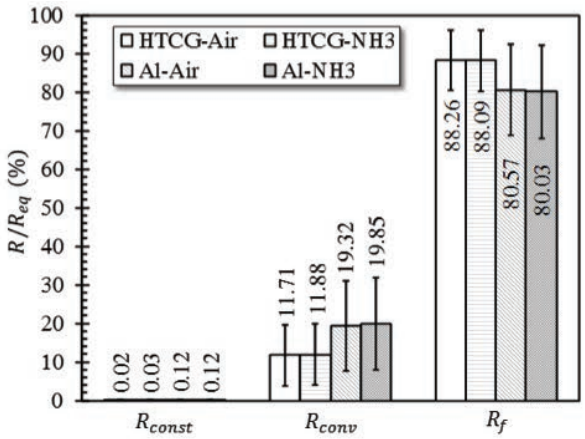

Figure 4 Relative importance of the main components of the equivalent thermal resistance when using dry air and ammonia gas as coolants and, aluminum and HTCG as bulk materials

In the same way, the high impact of R_f on the total thermal resistance and consequently on the heat transfer process can be noticed. This is due, including the basic assumptions made for the mathematical modeling construction, to the low density and low heat capacity of the working fluids. In order to have more illustrative examples of this behavior, some additional systems using the same rectangular microchannel were simulated, but changing the coolant to a nanofluid composed of titanium dioxide nanoparticles (9.0 wt/wt%) in water. The correlations and bulk properties required are not shown here, but they can be consulted in [18]. As can be noted from Figure 5, the impact of R_f on the total thermal resistance was drastically diminished, due to the relative high density and high heat capacity of the nanofluid, principally. Now the controlling factor in this case, is the convective resistance.

The modest increment of R_{const} is also evident. R_{conv} depends directly on the physical properties of the coolant, microchannel and the convective heat transfer coefficient, so there are a subtle balance of properties, which makes optimal the design and performance of a microchannel. The coupling of such properties makes the optimal design, without including the costs, a rather interesting real life problem. In a deeper analysis about the entropy generation for the system described above, Figure 6 shows the variation of Bejan number (*Be*) with the flow rate of the two working fluids, that is, TiO_2-water nanofluid, and water, for two different microchannels. As can be perceived, there is a sharp decrease of Bejan number when G_d increases. As soon as the volume flow rate of the working fluid reaches values above 0.007 m³/s, *Be* becomes practically zero. It

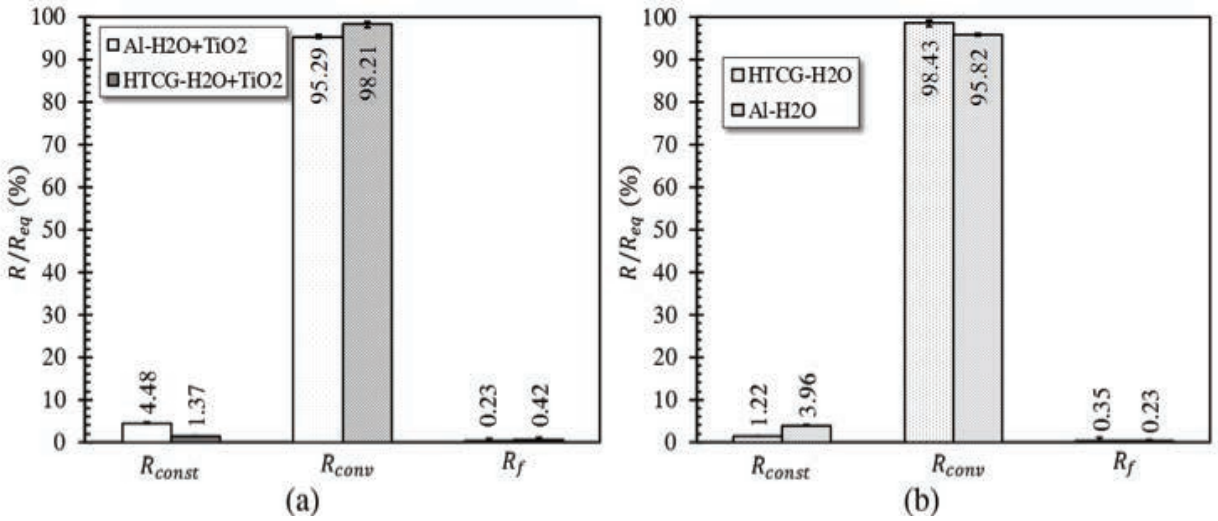

Figure 5 Relative importance of the main components of the equivalent thermal resistance when using two different types of coolant: (a) TiO_2-H_2O nanofluid, and, (b) water

could be interpreted as the continuous and dominant effect of the entropy generation due to the fluid friction on the heat transfer process.

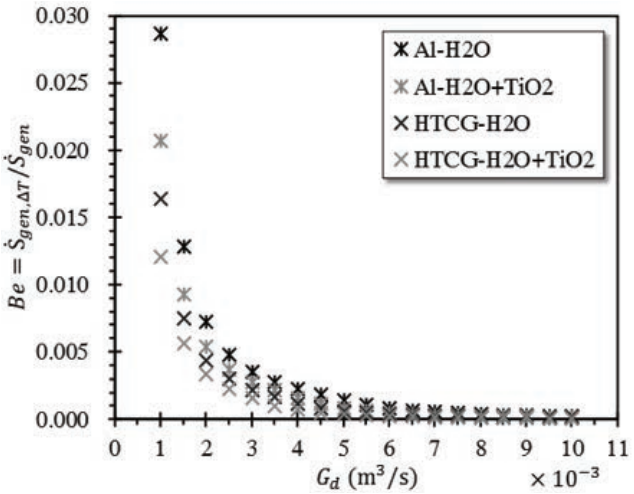

Figure 6 Bejan number (Be) and volume flow rate (G_d) relationship for different heat sinks materials and working fluids

On the other hand, the Nusselt number of the process was analyzed. It behaves as shown in Figure 7a. It seems that at higher flow rates of the working fluid, i.e. higher G_d, conduction is the dominant mechanism for heat transfer, or equivalently, the film coefficient seems to decrease with the length. This is more notorious when the material was a high thermal conductive graphite and air was the working fluid. Nevertheless, the changes were rather small. However, when the continuous phase is water the situation is different. Globally the Nusselt number is perceptibly lower, when the coolant is a nanofluid and the material for the making of the microchannel is a HTCG. It seems likely due to the dependence of the micro-flow hydrodynamics and the heat transfer process on the solid-liquid interfacial interactions, at such reduced length scales. Besides, it is currently known that the convective heat transfer coefficient is a function of the local velocity profile and could vary appreciably along the walls of the microchannel. Figure 7b shows the relation between pump power (Φ) and the equivalent thermal resistance (R_{eq}). Furthermore, it illustrates the relationship between the irreversibilities due to mass and heat transfer. The black arrow in this figure, represents the optimal design with the lowest value of $\dot{S}_{gen,min}$ for all the simulation scenarios analyzed.

It appears to be that a small change in the total or effective thermal resistance has a profound effect on the energy per unit time required to move the working fluid through the microchannel. Or in other words, any variation on the thermal resistant will alter the performance of the microchannel. The arrow represents minimum entropy generation rate at a specific volume flow rate G_d.

7. Conclusions

This article showed some of the most important results dealing with the use of one of the best material (a Higher Thermal Conductive Graphite) for making a heat sink, and its relative effect on the global heat transfer process. As can be initially concluded, it seems that the problem of heat transfer management on electronic components, using heat sinks with very high thermal conductivity (such as HTCG) and a gas as working fluid, comes from the side of the fluid. The thermal resistance and other surface properties imposed by the solid-fluid interphase appears to be the controlling mechanism for the overall heat dissipation, as well as, by the physicochemical properties of the coolant (density, heat capacity, viscosity, thermal conductivity and the eventual presence of another phases or components, principally). As it is evident, the next step is to find the kind of fluid or fluids that could markedly decrease the total thermal resistance.

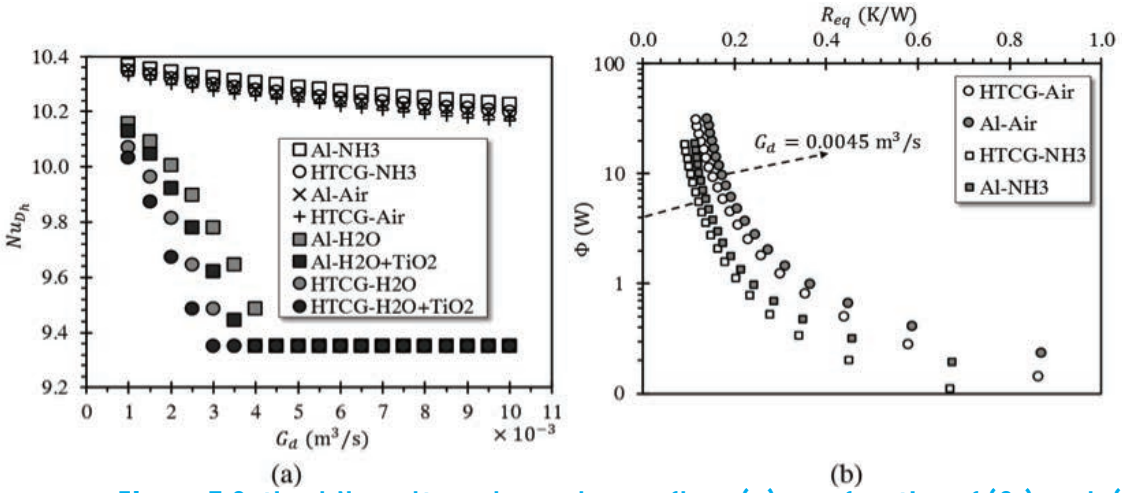

Figure 7 Optimal Nusselt number and pump flow: (a) as a function of (G_d), and, (b) as a function of (R_{eq})

Simulations results showed that a nanofluid composed of titanium dioxide and water, in conjunction with a high thermal conductive graphite is an acceptable combination to obtain a good performance microchannel.

8. Acknowledgements

The authors would like to express their gratitude to Vicerrectoría de Investigación y Extensión, at Universidad Industrial de Santander (Colombia), for the support granted through project 1807.

9. References

1. H. Fukushima, L. Drzal, B. Rook and M. Rich, "Thermal conductivity of exfoliated graphite nanocomposites", *J. Therm. Anal. Calorim.*, vol. 85, no. 1, pp. 235-238, 2006.
2. Hunan Chen Xiang Carbon Co., Ltd. (CX-CARBON), *Products*, 2014. [Online]. Available: http://www.cx-carbon.com/product/. Accessed on: Apr. 4, 2015.
3. S. Ghosh *et al.*, "Extremely high thermal conductivity of graphene: Prospects for thermal management applications in nanoelectronic circuits", *Appl. Phys. Lett.*, vol. 92, no. 15, pp. 15-17, 2008.
4. S. Kim and L. Drzal, "High latent heat storage and high thermal conductive phase change materials using exfoliated graphite nanoplatelets", *Sol. Energy Mater. Sol. Cells*, vol. 93, no. 1, pp. 136-142, 2009.
5. A. Tatami, M. Tachibana, T. Yagi, M. Akoshima and M. Murakami, "High Thermal Conductive Graphite Films from Thin Polymer Films", in *15th International Heat Transfer Conference*, Kyoto, Japan, 2014, p. 7.
6. C. Zhang, X. He, Q. Liu, S. Ren and X. Qu, "Fabrication and thermo-physical properties of graphite flake/copper composites", *J. Compos. Mater.*, pp. 1-8, 2014.
7. M. Mochane and A. Luyt, "The effect of expanded graphite on the thermal stability, latent heat, and flammability properties of EVA/wax phase change blends", *Polym. Eng. Sci.*, vol. 55, no. 6, pp. 1255-1262, 2015.
8. Y. Li, "Research on Expanded Graphite/Nitrate High-Temperature Composite Phase Change Materials", *Appl. Mech. Mater.*, vol. 740, pp. 11-14, 2015.
9. J. Luo *et al.*, "Numerical and experimental study on the heat transfer properties of the composite paraffin/expanded graphite phase change material", *Int. J. Heat and Mass Transf.*, vol. 84, pp. 237-244, 2015.
10. A. Adham, N. Mohd and R. Ahmad, "Optimization of an ammonia-cooled rectangular microchannel heat sink using multi-objective non-dominated sorting genetic algorithm (NSGA2)", *Heat and Mass Transf.*, vol. 48, no. 10, pp. 1723-1733, 2012.
11. A. Adham, N. Mohd and R. Ahmad, "Thermal and hydrodynamic analysis of microchannel heat sinks: A review", *Renew. Sustain. Energy Rev.*, vol. 21, pp. 614-622, 2013.
12. J. Cruz, I. Amaya and R. Correa, "Optimal rectangular microchannel design, using simulated annealing, unified particle swarm and spiral algorithms, in the presence of spreading resistance", *Appl. Therm. Eng.*, vol. 84, pp. 126-137, 2015.
13. W. Khan, M. Yovanovich and J. Culham, "Optimization of microchannel heat sinks using entropy generation minimization method", in *22nd Annual IEEE Semiconductor Thermal Measurement and Management Symposium*, Dallas, USA, 2006, pp. 78-86.
14. F. Incropera and D. DeWitt, *Fundamentals of heat and mass transfer*, 4th ed. New York, USA: John Wiley & Sons, 1996.
15. S. Kim and D. Kim, "Forced Convection in Microstructures for Electronic Equipment Cooling", *J. Heat Transfer*, vol. 121, no. 3, p. 639-645, 1999.
16. K. Parsopoulos and M. Vrahatis, "Unified Particle Swarm Optimization for Solving Constrained Engineering Optimization Problems", in *1st International Conference on Advances in Natural Computation* (ICNC), Changsha, China, 2005, pp. 582-591.
17. M. Kleiner, S. Kühn and K. Haberger, "High performance

forced air cooling scheme employing microchannel heat exchangers", *IEEE Trans. on Components, Packaging and Manuf. Technol., A*, vol. 18, no. 4, pp. 795-804, 1995.

18. N. Hajialigol, A. Fattahi, M. Ahmadi, M. Qomi and E. Kakoli, "MHD mixed convection and entropy generation in a 3-D microchannel using Al2O3–water nanofluid", *J. Taiwan Inst. Chem. Eng.*, vol. 46, pp. 30-42, 2015.